This is a repository copy of *Extracellular Vesicles Secreted by Human Adipose-derived Stem Cells (hASCs) Improve Survival Rate of Rats with Acute Liver Failure by Releasing lncRNA H19*.

White Rose Research Online URL for this paper:
http://eprints.whiterose.ac.uk/134486/

Version: Published Version

Article:

Research Paper

Extracellular Vesicles Secreted by Human Adipose-derived Stem Cells (hASCs) Improve Survival Rate of Rats with Acute Liver Failure by Releasing lncRNA H19

Qingchun Fu [a,*], Junyi Wang [b], Hongchao Li [b], Shane Gao [c], Rongfeng Shi [d], Danjing Yang [c], Xianli Wang [f], Xi Wang [a], Liang Zhu [c], Xiaojin Wang [b], Chengwei Chen [b], Ke Ning [e], Jun Xu [c,*], Zhengliang Gao [c,*], Yinpeng Jin [a,*]

[a] Shanghai Public Health Clinical Center, Fudan University, Jinshan, Shanghai 201508, PR China
[b] Shanghai Liver Diseases Research Center, The 85th Hospital of PLA, Shanghai 200235, PR China
[c] East Hospital, Tongji University School of Medicine, Shanghai 200120, PR China
[d] Department of Interventional & Vascular Surgery, Shanghai Tenth People's Hospital, Tongji University School of Medicine, Shanghai, 200072, PR China
[e] Department of Neuroscience, Sheffield Institute for Translational Neuroscience (SITraN), University of Sheffield, Sheffield, UK
[f] Institute of Neuroscience and State Key Laboratory of Neuroscience, Shanghai Institutes for Biological Sciences, Chinese Academy of Sciences, Shanghai, 200031, PR China

ARTICLE INFO

ABSTRACT

It has previously been reported that human adipose-derived stem cells (hASCs) can promote the regeneration of damaged tissues in rats with liver failure through a 'paracrine effect'. Here we demonstrate a therapeutic effect of hASCs derived Extracellular Vesicles (EVs) on rat models with acute liver failure, as shown by the improvement of the survival rate by >70% compared to controls. Gene sequencing of rat liver revealed an increase in human long-chain non-coding RNA (lncRNA) H19 after hASC-derived EVs transplantation. When the H19 coding sequence was silenced in hASCs and EVs were then collected for treatment of rats with liver failure, we saw a decrease in the survival rate to 40%, compared to treatment with EVs generated from non-silenced hASCs. These data indicate that lncRNA H19 may be a potential therapeutic target for the treatment of liver failure.

Research in context

Our research shows a therapeutic effect of hASCs derived Extracellular Vesicles (EVs) on rat models with acute liver failure, as demonstrated by a survival rate improvement of >70%. We speculate that hASCs derived Extracellular Vesicles promote hepatocytes' proliferation and improve the survival of rats with acute liver failure as a result of lncRNA H19 release.

1. Introduction

Liver failure poses a serious threat to the health of human beings. Orthotopic liver transplantation is currently the most effective treatment, but it is expensive and largely limited by the sources of the liver donors, making it unsuitable to serve as a common treatment method for the patients with end-stage liver failure ([1, 2]; Hessheimer et al., 2017). It has been shown that stem cells can promote the regeneration of impaired organs, tissues and cells through 'cell replacement' or the 'paracrine effect' ([4, 5, 53]; Jinglin et al., 2017; [7, 45]). As one of the adult stem cells, human adipose-derived stem cells (hASCs) are characterized by a high multiplication rate, broad differentiation potency and relatively easy accessibility, for which they are expected to be ideal seed cells for the treatment of some severe liver diseases such as acute liver failure (ALF) [8–10].

Originally, researchers held the view that stem cells repaired tissue injuries mainly through 'cell replacement' [11–13]; however, recent animal experiments have implicated that exogenous stem cells are largely eliminated by the recipient's immune system after a short period of time following in vivo transplantation, and very few stem cells differentiated into the functional somatic cells at targeted organs, suggesting that the therapeutic effect of transplanted stem cells may be attributable to their paracrine capacity [14–16]. Our findings in acute liver failure rat models show that hASCs facilitate the improvement of the rats' survival rate and liver function recovery, but the hepatocyte-related protein is not expressed within a short period of time after hASCs transplantation; as such, it can be predicted that the main active mechanism of

* Corresponding authors.
  E-mail addresses: qufu85@163.com (Q. Fu), xunymc2000@yahoo.com (J. Xu), zhengliang_gao@tongji.edu.cn (Z. Gao), 1182008211@qq.com (Y. Jin).

hASCs may result from the 'paracrine effect' rather than 'cell replacement' [4, 53].

HASCs can secrete proteins and RNA in the form of Extracellular Vesicles (EVs); the double-membrane structure of EVs can protect the internal protein and RNA from being degraded by various extracellular enzymes, and their functions can be exerted through interaction with the target cell surface receptors [17–20]. It has been reported that EVs isolated from BMSCs demonstrate better therapeutic effect in treating some heart and renal diseases in animal models than stem cells by promoting tissue repair and regeneration [21–28]. The efficacy of stem cell-derived EVs in treating acute liver injuries has also been reported [29, 30], however, the detailed mechanism remains unclear. In this study we obtained high-purity EVs from human adipose-derived stem cells. These EVs were then transplanted via the iliac vein into rats with acute liver failure, and a substantial therapeutic effect of hASCs-derived EVs was observed. We further explored the possible mechanism of hASCs-derived EVs in improving the outcomes of rats with acute liver failure through whole-genome RNA sequencing and bioinformatic analysis. We identified lncRNA H19, which was released by hASC-EVs, as a main target to exert the therapeutic effect by promoting hepatocytes' proliferation and viability of the rats with acute liver failure.

2. Materials and Methods

2.1. Isolation and Identification of hASCs

Adipose tissue was collected by liposuction from young healthy donors, which was approved by the ethical committee of the People's Liberation Army No. 85 Hospital, Shanghai, P.R. China (review serial number NO.2013/18). Relevant informed consent forms were signed by each donor before specimen collection. Adipose tissue was pulverized and cut into small pieces of about 1 mm³ after being washed three times in phosphate buffer solution (PBS) (Gibco, USA), and 0.1% collagenase I (Gibco, USA) was added for 30-minute digestion. A complete culture medium of an equal volume (DMEM-F12 culture medium (Hyclone, USA), 10% fetal calf serum (Gibco, USA)) was added to terminate digestion, and centrifugation was performed for 10 min at a rate of 1000 rpm. PBS solution was used to re-suspend the cells, which were then seeded into a T25 cell culture flask at a density of 1×10^6/ml after filtration through a 40 μm cell strainer and placed into a 37 °C and 5% CO_2 constant temperature incubator (Thermo, USA) for culture.

Surface molecular markers of hASCs were detected by flow cytometry as follows: hASCs of 2nd passage were collected into 3 tubes of 500 μl single-cell suspension, add 2 μl of anti-human CD44-FITC, CD90-FITC, CD73-FITC, CD19-FITC, CD34-FITC, CD45-FITC and CD105-PE monoclonal antibodies (eBioscience, USA) respectively, wash in PBS three times after a 30-minute incubation at 37 °C and use a flow cytometer (caliber, BD, USA) for detection.

2.2. Adipogenic/Osteogenic/Chondrogenic Differentiation

The P2 generation hASCs were seeded into six-well plates at a density of 5×10^3/cm² and cultured for three weeks in adipogenic/osteogenic/chondrogenic differentiation culture media. hASCs were washed in PBS for three times, fixed with 4% formalin for 10 min, incubated for 30 min with Oil Red O (Sigma, USA) or for 3 h with Alizarin bordeaux (Sigma, USA) or for 3 h with Alcian blue (HUXMA-90041; Cyagen Biosciences Inc.) at room temperature, and observed under a microscope after being washed in PBS for three times.

2.3. Isolation of hASCs-derived EVs

Culture medium of hASCs was collected and centrifuged at 3000 ×g for 15 min to remove cells and cell debris. The supernatant was transferred to a sterile vessel and an appropriate volume of ExoQuick-TC (System Biosciences, USA) was added to the biofluid and mixed by inverting or flicking the tube. The sample was kept in refrigerate overnight at 4 °C and centrifuged again at 1500g for 30 min next day. EVs were spinned down by centrifugating at 1500g for 5 min. All the supernant was discarded via aspiration. EV pellet was resuspended in 500 μl using PBS.

2.4. Characterization of hASCs-derived EVs

Firstly, we detected the physical shape of EVs using scanning electron microscope. One drop of hASCs-derived EVs (about 10 μg) was added onto the sealing membrane and forceps were used to cover the fluid drop with a carbon support film copper grid for five to ten minutes; then one drop of 2% phosphotungstic acid staining solution was added onto the sealing membrane and the copper grid was transferred from the drop of hASCs-derived EVs to the drop of phosphotungstic acid; after stained for three minutes, filter paper was used to absorb the liquid, the hASCs-derived EVs were baked under a filament lamp and observed with a transmission electron microscope.

The next, we detected the concentration and purification of EVs using Nanosight granulometer. The sample of hASCs-derived EVs was prepared in 1 ml of solution of a proper concentration. A Nanosight granulometer (NS300, UK) was used, the samples were injected into the sample cell, the suspension of hASCs-derived EVs was irradiated through the laser light source, the Brownian movement of the hASCs-derived EVs was observed with scattered light and the particle size distribution information of the hASCs-derived EVs was obtained. Then three-dimensional maps of the particle size were showed, corresponding quantitative distribution intensity and scattering intensity.

Then we used the Antibody Chip Reagent Kit (System Bioscience, USA) to test the surface markers of EVs. According to the instructions, the, 500 μg of hASCs-derived EVs protein was added to 500 μl of lysate, vortex mixing was performed for 15 s, 9 ml of EABB was added and mixed up and down for three times. 10 ml of the above mixture was added to the antibody chip and cultured overnight on a rocker at 4 °C. The mixture was abandoned, 10 ml of washing solution was added and kept stand on a rocker for 5 min at room temperature, the liquid was abandon, 10 ml of antibody mixture was added to the chip and kept stand on a rocker for 2 h at room temperature. The liquid was aspirated from the chip using a sheet of dry aspiration paper after washed for three times, mixed according to a 1:1 ratio so as to moderately develop the color of the liquid drops on the chips, and photos were taken under the chemiluminescence imaging system (LAS 4000 mini, GE, Japan).

The protein concentration of the EVs could be determined using BCA Protein Assay kit (Solarbio, Beijing, China). According to the instructions, the standard curve was plotted, the multi-gradient dilution of the hASCs-derived EVs were performed and seeded into a 96-well plate, 200 ml of BCA working solution was added to each well, the plate was kept stand for 15 to 30 min at 37 °C, and a multi-functional microplate reader (SoftMax Pro5, Molecular Devices, USA) was used to determine the absorbance value at a wavelength of A562 nm. The protein concentration was calculated according to the standard curve and sample data. The protein concentration of the EVs used in the subsequent tests was determined using this kit.

The amount of EVs could also be calculated by the expression of CD63 protein on surface of EVs. According to the instructions of the CD63 ELISA kit, 50 μl of protein standard and hASCs-derived EVs were added to a 96-well plate, and incubation was perform for two hours at 37 °C. After washed three times in a washing solution, 50 μl of EVs primary antibody was added and kept stand on a rocker for 1 h at room temperature. After washed three times in a washing solution again, 50 μl of EVs secondary antibody was added and kept stand on a rocker for 1 h at room temperature. After a third round of washing three times in a washing solution, 50 μl of TMB substrate was added and kept stand on a rocker for 30 min at room temperature; then 50 μl of stop buffer was added and the absorbance was detected using a multi-

functional microplate reader when the color in the well turns from blue to yellow.

To test if EVs could be uptaken by hepatocytes in vitro, we labelled the protein and RNAs in EVs and co-cultured the EVs with hepatocytes. In 500 μl of 1 μg/μl hASCs-derived EVs, the carboxyfluorescein succinimidyl diacetate ester (CFSE) and acridine orange were added in the 500 μl fluorescent labelling reagent kit (System Bioscience, USA). The well was mixed and kept stand for 10 min at 37 °C, ExoQuick antibody was added to terminate the fluorescence labeling, reversed upside down for six times and kept stand on ice for 30 min. Centrifuged at a rate of 14,000 rpm for 3 min, the supernatant was removed and 500 μl of PBS was added for dilution. The labeled EVs (100 μl per well) were added to the HL-7702 cells (human hepatocytes, Shanghai Linjiang Biotechnology Co., Ltd.) in the six-well plate and incubated for two hours. Then the uptake of the EVs by hepatocytes was observed under a fluorescent microscope.

2.5. Use of hASCs-derived EVs to Treat D-gal Induced ALF

Firstly, we established animal models with acute liver failure. Procedures involving animals and their care were conducted in conformity with animal ARRIVE guidelines and was approved by Animal Care and Use Committee of the Tongji University. 60 healthy male Sprague Dawley (SD) rats (130–150 g, grade:SPF, license: SCXK 2013-0005, SLAC Laboratory Animal Co., Ltd. (Shanghai, China)) at the age of 4–6 weeks were enrolled. The acute liver failure models were established by the two-time intraperitoneal injection of 0.8 g/kg D-aminogalactose with a 12-hour interval.

At 24 h after the establishment of acute liver failure rats models, the 60 rats were randomly divided into six groups: the group in which the rats received low-concentration of hASCs-derived EVs (20 μg/rat) via trans-iliac venous transplantation, the group in which the rats received high-concentration of hASCs-derived EVs (100 μg/rat), the group in which the rats received low-concentration of lysate (20 μg/rat), the group in which the rats received high-concentration of lysate (100 μg/rat), the hASCs (2×10^6 cells/rat) treated group and the PBS group as the control, and observe the 72-hour overall survival rate.

To observe the histopathological changes in rat's liver tissues, specimens from the peripheral sites of the hepatic portal vein were collected and embed in paraffin according to the conventional procedures, HE staining was performed and the hepatic histological manifestations was observed under a light microscope.

2.6. RNA sequencing analysis of rats' liver tissues

The rats' liver tissues were collected in the high-concentration hASCs-derived EVs transplantation group and PBS control group, TRIzol reagent was added to extract the RNA of the liver tissue, the total quantity was measured using an RNA quantitative device and preserved it in a − 80 °C refrigerator; a cDNA bank was established for the RNA with an RIN value of >8.0 as measured, the RNA sequence was detected on a ProtonTm system platform using the high-flux sequencing method and a corresponding RNA sequence heatmap was shown. The measured RNA sequences were compared with the human and rat RNA banks, and the differences between these two groups were found in terms of human and rat's RNA expression.

To analysis these signal pathways, all detected RNA sequences were retrieved in the KEGG database in the form of FASTA (http://geneontology.org/), important signal pathways were selected by means of the FISHER exact test and the *P* value was corrected using the Benjamini-Hochberg method; the significance is only considered in case $P < 0.05$ and in the presence of functional gene categories and pathways.

To analysis the role of signal pathways in the network, the important signal pathways of the bodies involved in all RNAs were prepared as detected in the netgraphs, the selected genes were genes with abundant content in the pathways ($P < 0.05$) and the position of each signal pathway in the network and their mutual relationships were observed.

Then we use RT-qPCR for in vitro validation, the hASCs-derived EVs were lysed using TRIzol and the expression of the drug metabolism signal pathway related genes were detected using RT-qPCR.

2.7. Role of lncRNA H19 in hASCs-derived EVs

To verify the role of H19 in EVs, we collected the hASCs-derived EVs with silenced lncRNA H19. The H19 shRNA (Accession number: 5′-3′ GCAAGAAGCGGGTCTGTTTCT)-carrying plasmid pGLV3/H1/GFP + Puro Vector was constructed, packed in the lentivirus and used to infect the hASCs, the hASCs with silenced H19 genes were harvested and the EVs were collected. RT-qPCR was used to detect the expression of lncRNA H19 in hASCs-derived EVs before and after silencing.

The next, In vitro proliferation test of human hepatocytes (HL-7702) was performed when co-cultured with EVs, human hepatocytes were seeded in a 96-well plate at the rate of 5000 cells/well; after the cells became adherent, the hASCs-derived EVs and hASCs-derived EVs with silenced H19 genes were added to the blank plates according to different concentrations, CCK8 reagent was added at the rate of 10 μl at different time points and incubated for 30 min; then the A450 value was detected and the respective impact of the two groups of hASCs-derived EVs on the proliferation of human hepatocytes were evaluated.

Then we transplanted the hASCs-derived EVs of the silenced H19 gene and observed the 72-hour overall survival rate. 30 healthy male SD rats (130–150 g, grade:SPF, license: SCXK 2013–0005, SLAC Laboratory Animal Co., Ltd. (Shanghai, China)) at the age of 4–6 weeks were enrolled. All animal ARRIVE guidelines have been met. The acute liver failure models were established by the two-time intraperitoneal injection of 0.8 g/kg D-aminogalactose with a 12-hour interval. At 24 h after the model establishment, the rats were randomly divided into three groups: the group in which the rats received hASCs-derived EVs (100 μg/rat) via the trans-iliac venous transplantation, the group in which the rats received the hASCs-derived EVs of the silenced H19 gene (100 μg/rat) and the PBS control group, and the 72-hour overall survival rate was observed.

2.8. Use of hASCs-derived EVs to Treat D-gal + LPS Induced ALF

We further established a more severe ALF model with D-gal + LPS to observe the inflammatory status in rats when treating with EVs. 21 healthy male SD rats (130–150 g, grade:SPF, license: SCXK 2013-0005, SLAC Laboratory Animal Co., Ltd. (Shanghai, China)) at the age of 4–6 weeks were enrolled. All animal ARRIVE guidelines have been met. The acute liver failure models were established by intraperitoneal injection of 0.8 g/kg D-aminogalactose and 5 μg/kg LPS.

At 2 h after the establishment of the acute liver failure rate models, the 21 rats were divided into two groups: the group in which the rats received high-concentration hASCs-derived EVs (100 μg/rat) (10 rats) via trans-iliac venous transplantation and the group in which the rats received PBS (11 rats), and the 72-hour overall survival rate and histopathological changes in rat's livers tissues was observed.

To detect rats' liver function indicators, the rat's serum was collected 1 day after the transplantation and a blood biochemical analyzer was used to detect the concentrations of ALT, AST and LDH in the rat serum.

We also collected rat's serum for protein chip detection, at 1 day after the transplantation, a qualitative analysis of the expression of such inflammatory factors as IL-1ra, IL-1α and IL-1β, and such chemotactic factors as CCL3, CCL5 and CCL20 was made, in the rat serum using the rat cytokine protein chip method (R&D, ARY008). Photos were taken using a gel imaging system (GE, LAS4000 mini) and the Mean Pixel Density was analyzed using HLImage software.

2.9. Underlying Mechanism of lncRNA H19 on Hepatocytes

From the RNA sequencing analysis above, we also found an up-regulation of HGF/c-Met pathway. So, RT-qPCR was use to verify the expression of HGF and c-Met in rats' liver before and after transplantation of high-concentration hASCs-derived EVs.

To verify the role of H19 in EVs, we collected the hASCs-derived EVs with overexpressed lncRNA H19. The H19-carrying plasmid GV461 (CMV-betaGlobin-MCS-SV40 PolyA) Vector was constructed, packed in the adenovirus (AAV) and used to infect the hASCs, the hASCs with overexpressed H19 genes were harvested and the EVs were collected. RT-qPCR was used to detect the expression of lncRNA H19 in hASCs-derived EVs before and after overexpressing.

Then, we detected hepatocytes' proliferation with the CCK8 kit. The cells were divided into four groups: H19-EVs, AZD6094-EVs, EVs and control. The hepatocytes were inoculated in a 96-well plate with a cell density of 2000 cells/well. 24 h later, 8 mg/ml D-gal and 0.05 μg/ml LPS were added into the culture medium; for the AZD6094-EVs group, an additional 0.8 mg/ml of c-Met kinase inhibitor AZD6094 (AZD6094 is a type of ATP-competitive c-Met inhibitor which may block the signal transduction of the HGF/c-Met pathway) was added. 24 h later, 1 μg/ml of hASCs-derived EVs with an overexpression of H19, hASCs-derived EVs, hASCs-derived EVs and PBS were added to the groups respectively. CCK8 reagent was added at 2 h, 24 h, 48 h, 72 h, and 96 h and incubated at 37 °C for 1 h and the OD at a wavelength of 450 nm was detected with a multi-function microplate reader.

The next, we detected hepatocytes' apoptosis with the TUNEL kit, the cells were divided as above, cultured at 37 °C for 24 h and fixed for 30 min in 4% paraformaldehyde and implement PBS cleaning. Then the primary antibodies and secondary antibodies were sealed and incubated, DAPI was added and sealed the slides. Finally, the hepatocyte apoptosis was observed under an upright fluorescence microscope.

We also detected hepatocytes' apoptosis with flow cytometry, the cells were divided as above, cultured at 37 °C for 24 h and digested for 3 min in 0.25% trypsin. To prepare single-cell suspension, 100 μl of suspension was taken, 3 μl of Annexin V-FITC and PI were added and placed at room temperature for 30 min, The appropriate amount of 1× buffer was added and finally apoptosis conditions were detected with a flow cytometer.

Again, animal models with acute liver failure were established, 30 healthy male SD rats (130–150 g, grade:SPF, license: SCXK 2013–0005, SLAC Laboratory Animal Co., Ltd. (Shanghai, China)) at the age of 4–6 weeks were enrolled. All animal ARRIVE guidelines have been met. The acute liver failure models were established by intraperitoneal injection of 0.8 g/kg D-aminogalactose and 5 μg/kg LPS.

At 2 h after the establishment of the acute liver failure rate models, the 40 rats were divided into four groups: the group in which the rats received hASCs-derived EVs with an overexpression of H19 (100 μg/rat) (10 rats) via trans-iliac venous transplantation, the group in which the rats received hASCs-derived EVs (10 rats), the group in which the rats pretreated with AZD6094 and received hASCs-derived EVs (10 rats) and the group in which the rats received PBS (10 rats), and the 72-hour overall survival rate was observed.

Then, Ki67 immunohistochemical staining of was performed to verify the regeneration of rat's liver tissues. Paraffin imbedding was carried out for the hepatic tissue, then sliced and deparaffinated the tissue, repaired the antigen and incubated the primary and secondary antibodies. DAB coloration, transparency, slice sealing and conventional immunohistochemical treatment were conducted. The hepatic proliferation was observed under a microscope.

Correspondingly, hepatic apoptosis was detected using the TUNEL kit. Paraffin imbedding was carried out for the hepatic tissue, then sliced and deparaffinated the tissue, repaired the antigen, sealed and incubated the primary and secondary antibodies. Later, DAPI, slice sealing and conventional immunohistochemical treatment were conducted.

Finally, the hepatic apoptosis was observed under an upright fluorescence microscope.

Finally, we detected the expression of HGF, c-Met, STAT3 and PI3K of hepatic tissue using RT-qPCR. Hepatic tissues were taken from rats in each group, RNAs were extracted with TRIzol, cDNA was formed through reverse transcription and the gene expression quantity of HGF, c-Met, STAT3 and PI3K were detected through real-time fluorescence quantification PCR.

2.10. Statistical Data and Analysis

The experimental data was statistically analyzed using the SPSS 19.0, and the indicators of the measurement data were expressed using the mean ± standard error (X ± SEM). The Kaplan-Meier method was adopted for the survival analysis, with $P < 0.05$ meaning a statistically significant difference.

3. Results

3.1. Isolation and Identification of hASCs

The hASCs was cultured up to five passages as previously reportedly [4, 53]. The hASCs showed typical spindle-like structures without obvious changes in shape, size or density (Fig. S1A). These hASCs had a high percentage of positive expression of mesenchymal stem cells markers such as CD73 (100%), CD44 (100%), CD90 (99.9%), CD105 (97.2%), etc. and nearly no expression of hematopoietic cell line molecular markers such as CD34, CD45 and CD19 (0.8%) by the flow cytometry (Fig. S1B). Three-lineage differentiation assay was performed to test the multiple potency of hASCs. After culturing for three weeks on agar medium, massive amounts of lucent lipid droplets of a high refractivity could be visualized in the cytoplasm as observed under a microscope, and the color red was developed after using Oil Red O for staining; after a three-week osteogenic/chondrogenic medium culture, the cells were stained using Alizarin bordeaux/Alcian blue and the majority of the cells were stained red/blue as observed under the microscope (Fig. S1C). These results indicated that we obtained hASCs with high purity and multi-differentiational ability.

3.2. Characterization of hASCs-derived EVs

hASCs-derived EVs were isolated using ExoQuick-TC kit and EVs were characterized by a scanning electron microscope (SEM) and a Nanosight granulometer. Under SEM, the hASCs-derived EVs could be visualized with saucer-like or concave-hemispheric structures and relatively similar sizes ranged from about 30 to 150 nm (Fig. 1A). When using a Nanosight granulometer to detect the hASCs-derived EVs, the dimension/concentration curve showed that the hASCs-derived EVs had dimensions of about 30 to 150 nm with a mean of about 100 nm, and the sample concentration was 4×10^7 particles per ml. As shown in the dimension/intensity curve, the hASCs-derived EVs had an intensity of about 0.5 to 6 a.u., and the particles with dimensions of about 150 nm had the highest intensity. As shown in the dimension/concentration/intensity three-dimensional graphics, the hASCs-derived EVs had a relatively high purity within the dimension range of 80 to 120 nm. In addition, the Brownian movement of the hASCs-derived EVs in the fluid could be captured by means of a granulometer (Fig. 1B). Surface markers of hASCs-derived EVs were detected by protein chip assays. The majority of protein markers for EVs including CD81, ANXA5, ICAM, ALIX, TSG101, FLOT1, CD63 and GM130 were detectible (Fig. 1C).

The factors which might affect the yield of hASCs-derived EVs were analyzed by a Nanosight granulometer and the ELISA assay. The protein concentration of the collected hASCs-derived EVs was positively correlated with the quantity of EVs (Fig. 1D). These results indicated that the confluence of hASCs culture, cell generation (within the fourth generation), cell quality (visual measurement method) and times of culture
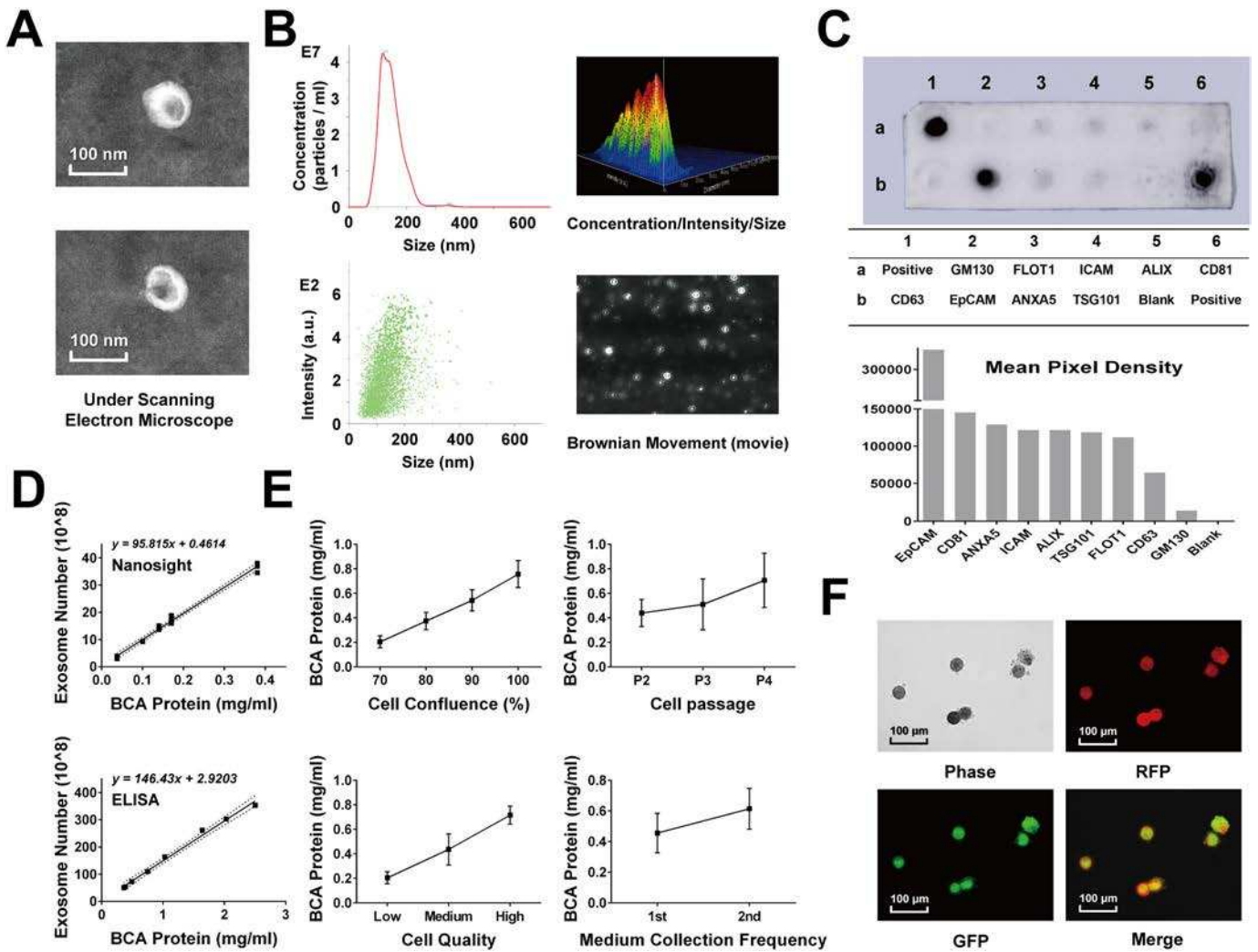
Fig. 1. Identification of hASCs-derived EVs. (A) Observation under electron microscope: the hASCs-derived EVs appeared globular with a size ranging from about 30 to 150 nm. (B) The physical parameters of the hASCs-derived EVs were detected using the Nanosight granulometer, the curve described the relationship between particle size (X axis) and concentration/intensity distribution (Y axis), and it was visible that the size of most hASCs-derived EVs ranged from 30 to 150 nm; the Brownian movement of the hASCs-derived EVs in liquid could be visualized. (C) The common surface protein markers of the hASCs-derived EVs were detected by the protein chip method, and ImageJ software was used to calculate the mean grey level. (D) Detection was performed using a Nanosight granulometer and the ELISA method, and the protein content of the collected hASCs-derived EVs was positively correlated with the quantity of EVs. (E) The hASCs fusion degree, cell generation, cell quality and times of culture medium collection was positively correlated with the protein content of the EVs (BCA protein determination method). (F) Red or green fluorescence was displayed after the hepatocellular uptake of the EVs under a fluorescence microscope, indicating the presence of RNA or proteins in the EVs. (For interpretation of the references to color in this figure legend, the reader is referred to the web version of this article.)

medium collection (within two times) were positively correlated with the protein concentration of the EVs (BCA Protein Assay method) (Fig. 1E).

To test whether the EVs could be uptaken by hepatocytes, hASCs-derived EVs were labelled by GFP and RFP for EV-specific protein and RNA respectively. Then hASCs-derived EVs were incubated with hepatocytes for two hours. GFP and RFP-positive particles could be simultaneously visualized within the hepatocellular cytoplasm (Fig. 1F), and both green and red fluorescence didn't become dimmer over time, implying that hASCs-derived EVs could penetrate hepatocellular membranes, enter hepatocellular cytoplasm and exist in hepatocytes for a relatively long period of time.

3.3. hASCs-derived EVs Can Significantly Rescue D-galactosamine (D-gal) Induced Acute Liver Failure (ALF)

As previously reported, hASCs can partially rescue the ALF. We further explored whether the effect of hASCs on ALF is mainly achieved through EVs. The ALF rat model was made by the intraperitoneal injection of D-gal. One day after establishing the ALF disease model, the rats received an injection of low-concentration hASCs-derived EVs (20 μg/rat), high-concentration hASCs-derived EVs (100 μg/rat), low-concentration lysate (20 μg/rat), high-concentration lysate (100 μg/rat), hASCs (2 × 10^6 cells/rat) and PBS via the iliac vein, and the overall survival rates were 62.5%, 100%, 25%, 50%, 37.5% and 27.3% respectively. When comparisons were made between the high and low-concentration EVs transplantation groups and the control group, the survival rates at different time points presented significant differences ($P < 0.05$) (Fig. 2A). These results indicated that hASCs-derived EVs can rescue the ALF and this therapeutic effect is relative to their concentration.

To observe the histology change of rat's liver, HE staining was performed on the hepatic tissues at 24 h after transplantation. As observed under an optical microscope, a large area of degeneration and necrosis could be visualized in rats' liver in the high and low-concentration hASCs lysate transplantation groups, the hepatic sinus became dilated and massive inflammatory cell infiltration could be visualized in the portal area and necrotic area; as for the rats in the
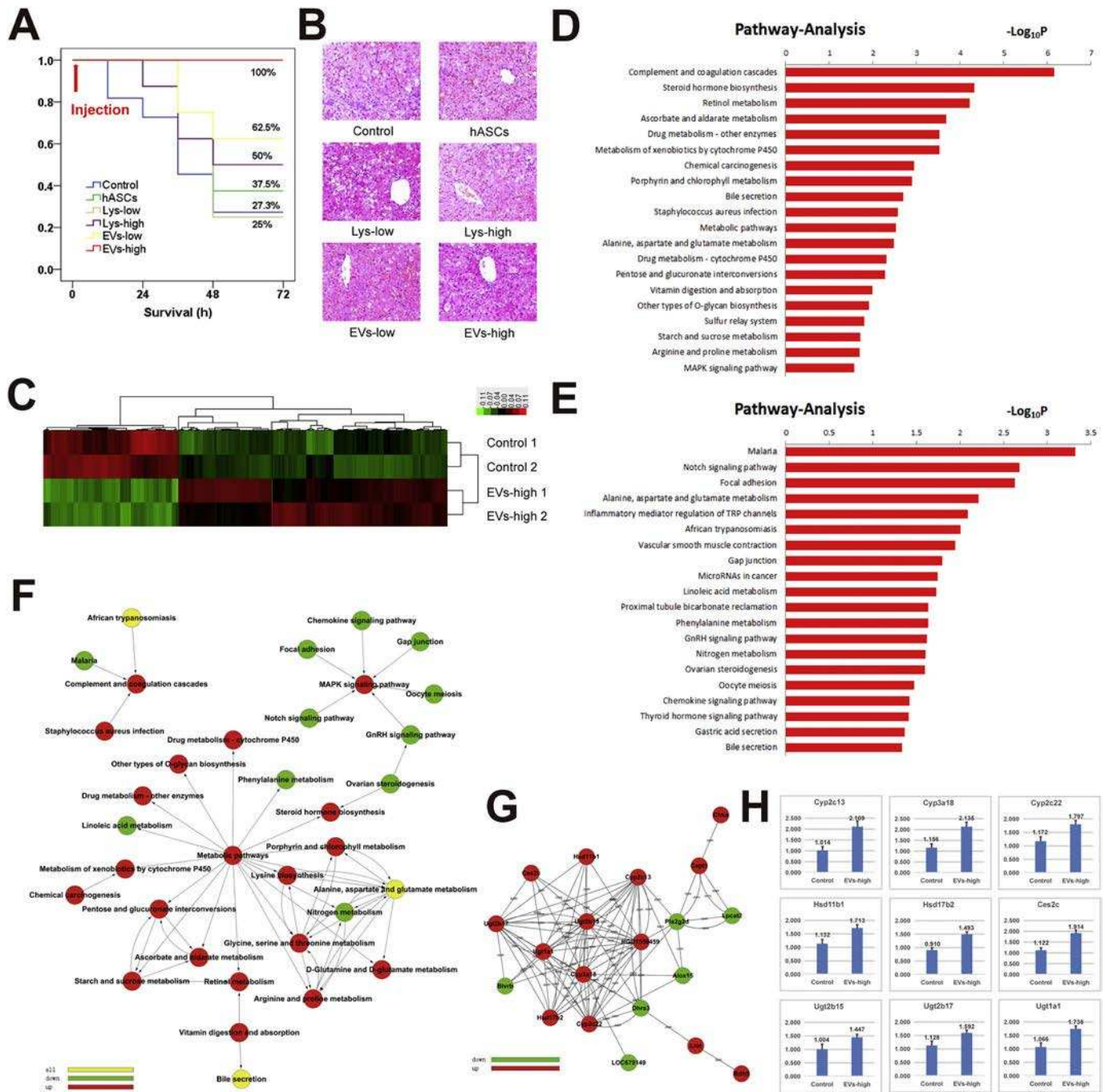
Fig. 2. hASCs-derived EVs rescue D-gal induced ALF. (A) The 72-hour survival rates of high-concentration and low-concentration hASCs-derived EVs transplantation groups ('EVs-high' and 'EVs-low'), high-concentration and low-concentration hASCs lysate transplantation group ('Lys-high' and 'Lys-low'), hASCs transplantation group and PBS control group was observed. The comparison between the EVs-high and EVs-low groups and the control group showed significant differences in terms of survival rates at different time points ($P < 0.05$). (B) The paraffin sections of the liver tissues of rats in each group were prepared, and photos taken under a microscope after HE staining (400×). (C) The liver tissues of the rats in the EVs-high group and the control group were collected and homogenized, then second-generation gene sequencing was performed to create a heatmap. (D) The KEGG signal pathway analysis of the sequencing results showed that, when compared with the control group, there was an up-regulation in pathways such as coagulation cascades, drug metabolism and MAPK Signaling in the EVs-high group. (E) There was a down-regulation in pathways such as inflammatory mediator regulation of the TRP channels and chemokine signaling pathway. (F) Through signal network analysis, after high-concentration hASCs-derived EVs treatment, such up-regulated signal pathways as complement, hemagglutination, drug metabolism and MAPK signaling were at the core positions in the entire signal pathway network (red represents up-regulated genes and green represents down-regulated genes). (G) The related enzymes involved in drug and poison metabolism in the drug metabolic pathway were clearly up-regulated. (H) The results of RT-qPCR detection re-validated the sequencing results. (For interpretation of the references to color in this figure legend, the reader is referred to the web version of this article.)

high-concentration hASCs-derived EVs transplantation group, the hepatic structures of their hepatic lobules and hepatic sinus basically recovered to normal, with only a small amount of infiltrated inflammatory cells detectable. (Fig. 2B). These results indicated that the transplantation of hASCs-derived EVs reduced the necrosis and inflammation in rats' liver.

3.4. The Main Signaling Pathway, Which May Have Impact on the Therapeutic Effect of hASCs-derived EVs is Unraveled by Whole-genomic Sequencing and Bioinformatic Analysis

To explore the mechanism of hASCs-derived EVs in rescuing rats with ALF, the RNA of rats' hepatic tissues in the high-concentration
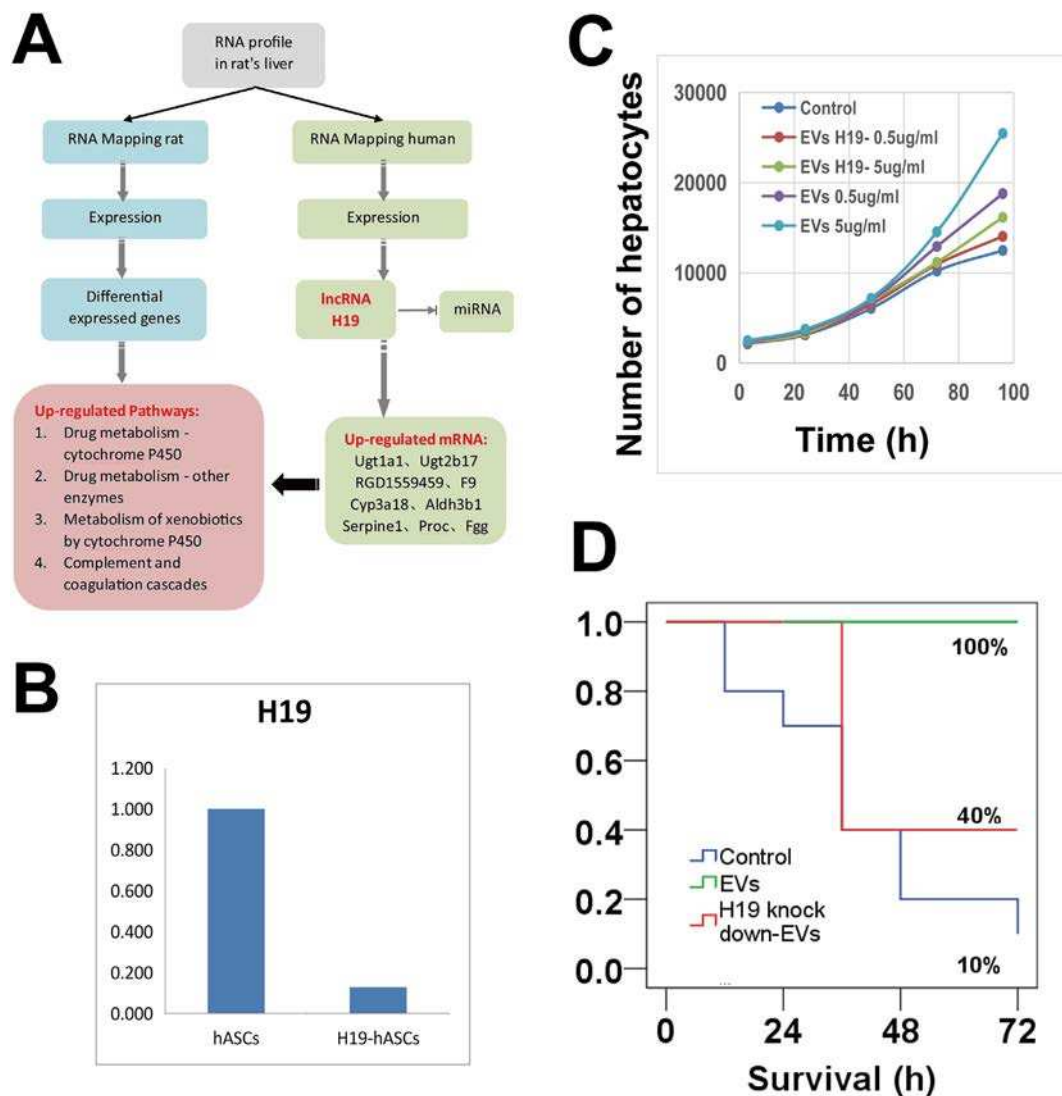
Fig. 3. Function of lncRNA H19 on hepatocytes. (A) After a comparison between the RNA sequencing results and human and rat gene banks, it was found that there was an up-regulation in the human-derived long-chain non-coding RNA H19 gene measured in the hepatic tissues of the rats in the hASCs-derived EVs group. (B) The expression of lncRNA H19 in the hASCs-derived EVs became clearly down-regulated after the H19 gene was silenced. (C) hASCs-derived EVs with silenced H19 genes had no promotional effects on the proliferation of hepatocytes. (D) The rats in the hASCs-derived EVs group and hASCs-derived EVs with silenced H19 gene group presented significant differences in terms of their survival rates at different time points ($P < 0.05$).

hASCs-derived EV transplantation group and control group was sequenced simultaneously. From the heatmap, it was clearly evident that the injection of high-concentration hASCs-derived EVs could impact the RNA expression of rat' liver tissues when compared with the control group (Fig. 2C). After conducting a KEGG signal pathway analysis of the sequencing results, it was noted that when compared with the control group, after the injection of the high-concentration hASCs-derived EVs, some important intrahepatic signal pathways which are essential for maintaining the normal liver function, such as coagulation cascades, drug metabolism and MAPK signaling were up-regulated (Fig. 2D). Nonetheless, some signaling pathways which may affect the inflammatory status of the liver, such as the inflammatory mediator regulation of the TRP Channels and chemokine signaling pathway became down-regulated (Fig. 2E). The network of the main signaling pathways was further analyzed by Pathway-Act-Network analysis. Consistent with KEGG signal pathway analysis, the rats in the high-concentration EVs transplantation group also showed the significant up-regulation of such signal pathway-related genes as coagulation cascades, drug metabolism and MAPK Signaling, which were at the core position in the entire signal pathway network (Fig. 2F). The related enzymes involved in drug and poison metabolism, such as Cyp2c13,

Hsd11b1, Ugt2b15 et al., were clearly up-regulated (Fig. 2G) and the RT-qPCR results re-validated the sequencing results (Fig. 2H).

3.5. Role of lncRNA H19 in hASCs-derived EVs

After a comparison between the RNA sequencing results and human and rat gene banks, an up-regulation was found in the human-derived long-chain non-coding RNA H19 gene measured in the hepatic tissues of rats in the hASCs-derived EVs group. Software was used to predict the microRNA that might interact with human lncRNA H19, and it was found that lncRNA H19 happened to be closely associated with the microRNA of coagulation functions, drug metabolism, etc. pathways. We also found in the previous RNA sequencing results that there was an up-regulation in genes related to the coagulation function and drug metabolic pathways in rat hepatic tissues. As such, it was assumed that hASCs-derived EVs are very likely to inhibit the expression of microRNA related to the coagulation function, drug metabolism, etc. pathways in rats, thus up-regulating such pathways and improving the survival rate of rats with ALF (Fig. 3A).

To explore the role of lncRNA H19 in hASCs-derived EVs, we silenced H19 genes in hASCs and collected the EVs for in vitro and in vivo

experiment. RT-qPCR was used to detect the expression of lncRNA H19 in hASCs-derived EVs before and after silencing. As shown in RT-qPCR detection, the expression of lncRNA H19 in hASCs-derived EVs became clearly down-regulated after the H19 gene was silenced (Fig. 3B).

In vitro experiment, we co-cultured the EVs and hepatocytes, as shown in CCK8 detection, hASCs-derived EVs can promote human hepatocellular proliferation, nevertheless, hASCs-derived EVs with silenced H19 genes lost their promotional effects which indicated that H19 may be crucial in the promotion process of hepatocellular proliferation (Fig. 3C).

In vivo experiment, we also observed the 72-hour overall survival rate of rats treating with hASCs-derived EVs with silenced H19 genes. At 1 day after model establishment through the intraperitoneal injection of D-gal, rats receiving the injection of hASCs-derived EVs (100 μg/rat), hASCs-derived EVs with the silenced H19 gene (100 μg/rat) and PBS via the iliac vein had 72-hour overall survival rates of 100%, 40% and 10% respectively. The rats' survival rates in the hASCs-derived EVs group and the hASCs-derived EVs with silenced H19 gene group presented significant differences at different time points ($P < 0.05$) (Fig. 3D). These results indicated that H19 may be crucial in promoting hepatocellular proliferation and thus rescuing rats with ALF.

3.6. hASCs-derived EVs Rescue D-gal + Lipopolysaccharide (LPS) Induced ALF

From the experiments above, we found that hASCs-derived EVs could promote hepatocellular proliferation and rescue rats with D-gal induced ALF. To further verify the therapeutic effect of EVs, we established a more severe and fatal model of ALF using D-gal and LPS. At 2 h after model establishment through the intraperitoneal injection of D-gal + LPS, the rats received an injection of high-concentration hASCs-derived EVs (100 μg/rat) and PBS via the iliac vein, and the 72-hour overall survival rates were 50% and 9% respectively; the rats in the two groups presented significant differences in terms of the survival rates at different time points ($P < 0.05$) indicating that hASCs-derived EVs also had therapeutic effect in D-gal + LPS induced ALF (Fig. 4A).

Histology examination showed that the rats in the PBS control group had damaged hepatic lobule structures, dilated hepatic sinuses with congestion and bleeding, and massive inflammatory cell infiltration could be visualized in the portal area and necrotic area; as for the rats in the hASCs-derived EVs transplantation group, the structures of their hepatic lobules and hepatic sinuses basically recovered to normal, with only a small amount of inflammatory cell infiltration visible which indicated that hASCs-derived EVs may improve the inflammatory status in rats' liver (Fig. 4B).

Also, the level of Alanine aminotransferase (ALT), Aspartate aminotransferase (AST) and Lactate Dehydrogenase (LDH) in rats' serum were detected for evaluation of rats' liver function. At 24 h after transplantation, the rats in the hASCs-derived EVs transplantation group had a significantly lower level of ALT [(7091.4 ± 3473.9) U/L] than those in the control group [(10,615 ± 2950.8) U/L], lower level of AST [(7627.5 ± 3822.5) U/L] than those in the control group [(16,163.8 ± 4660.6) U/L]; and lower level of LDH [(62,476.3 ± 32,829.8) U/L] than those in the control group [(83,902.5 ± 17,114.3) U/L] ($P < 0.05$) (Fig. 4C). These results indicated that hASCs-derived EVs contributed to the recovery of rats' liver function.

To clearly investigate the inflammatory status in rats' liver, we harvested rat serum for protein chip detection. At 1 day after transplantation, the rats in the hASCs-derived EVs transplantation group had a lower level of such inflammatory factors in the rat serum as IL-1ra, IL-1α, IL-1β, IL-6 and IL-17 than those in the PBS control group; and a lower level of such chemotactic factors as CCL20, CINC-1, CINC-2α/β, CINC-3, CNTF, CX3CL1, CXCL7, CXCL9, CXCL10 and LECAM-1 than those in the PBS control group indicating that hASCs-derived EVs also have some anti-inflammatory effect (Fig. 4D).

3.7. Underlying Mechanism of lncRNA H19 in Treating D-gal + LPS Induced ALF

From the RNA sequencing analysis above, we also found an up-regulation of HGF/c-Met pathway and this was verified in the liver tissue of rats using RT-qPCR method (Fig. S2A). HGF/c-Met pathway is a well-known pathway associated to cells proliferation. To explore the role of HGF/c-Met pathway in rats treating with EVs, we constructed the adenovirus (AAV) overexpressing H19, infected hASCs and collected their EVs. RT-qPCR was used to detect the expression of lncRNA H19 in hASCs-derived EVs before and after overexpressing. As shown in RT-qPCR detection, the expression of lncRNA H19 in hASCs-derived EVs became clearly up-regulated after the H19 gene was overexpressed (Fig. S2B). In vitro experiment, we found that hASCs EVs with an over-expression of H19 (H19-EVs) promoted hepatocytes' proliferation, which hints that H19 can further enhance the role of hASCs-derived EVs in promoting hepatocytes' proliferation. Then the c-met inhibitor — AZD6094 was used to block HGF/c-Met pathway in hepatocytes. After pretreatment with AZD6094, hASCs-derived EVs lost their effect on promoting hepatocytes' proliferation, which indicated that hASCs-derived EVs may promote hepatocytes' proliferation through the HGF/c-Met pathway (Fig. S3A).

We also found that lncRNA H19 reduced hepatocytes' apoptosis in vitro. The apoptosis rate of the H19-EVs group is lower than that of the EVs group, which indicates that H19 can enhance the protective effect of EVs on hepatocytes, thus reducing drug-induced hepatocytes' apoptosis. The apoptosis rate of the AZD6094-EVs group is higher than that of the EVs group, which indicates that hASCs-derived EVs may reduce hepatocytes' apoptosis through the HGF/c-Met pathway (Fig. S3B). H19-EVs, EVs, AZD6094-EVs and control groups had late apoptosis rates of 10.6%, 12.1%, 24.8% and 26.5% respectively. The apoptosis rate of H19-EVs is lower than those of the other three groups, which indicated that H19 can reduce the toxic effects of D-gal and LPS on hepatocytes, thus improving the role of EVs in apoptosis inhibition (Fig. S3C).

In vivo experiment, hASCs-derived EVs promoted hepatocytes' proliferation in damaged liver tissues, and H19 further enhanced the role of EVs in promoting hepatocytes' proliferation. The number of brown nuclei in the AZD6094 intervention group was slightly lower than that of the hASCs-derived EVs group, which indicated that hASCs-derived EVs may promote the regeneration of rats' liver through the HGF/c-Met pathway (Fig. S3D, F).

Then we detected the hepatic apoptosis in the hepatic tissues of rats with the TUNEL kit and found that lncRNA H19 reduced the apoptosis of rats' liver. The number of apoptotic cells of the H19-EVs group is significantly lower than that of the hASCs-derived EVs, AZD6094-EVs and control groups, which indicated that hASCs-derived EVs could reduce the damage of hepatic tissues caused by D-gal + LPS, and H19 can enhance the protective effects of EVs on hepatocytes. The apoptosis degree of the AZD6094-EVs group is greater than that of the hASCs-derived EVs group, which indicated that EVs may protect hepatocytes and reduce the apoptosis of rats' liver through the HGF/c-Met pathway (Fig. S3E, F).

The 72-hour overall survival rates of the H19-EVs, AZD6094-EVs, EVs and control groups were 80%, 20%, 50% and 10% respectively; the rats in the H19-EVs and control groups presented significant differences in terms of their survival rates at different time points, while the rats in the AZD6094-EVs and EVs groups likewise presented significant differences in terms of their survival rates at different time points (Fig. S3G).

To explore the mechanism of H19 in influencing HGF/c-Met pathway, we detected the gene expression quantity of HGF, c-Met, STAT3 and PI3K of hepatic tissue using RT-qPCR. The gene expressive quantity of HGF, STAT3, and PI3K in the liver tissues of the rats in the AZD6094-EVs group were lower than those in H19-EVs and EVs groups, which indicated that hASCs-derived EVs could promote hepatocytes' proliferation through up-regulating the expressions of HGF, STAT3, and PI3K. However, the expressions of HGF, STAT3 and PI3K are all restrained
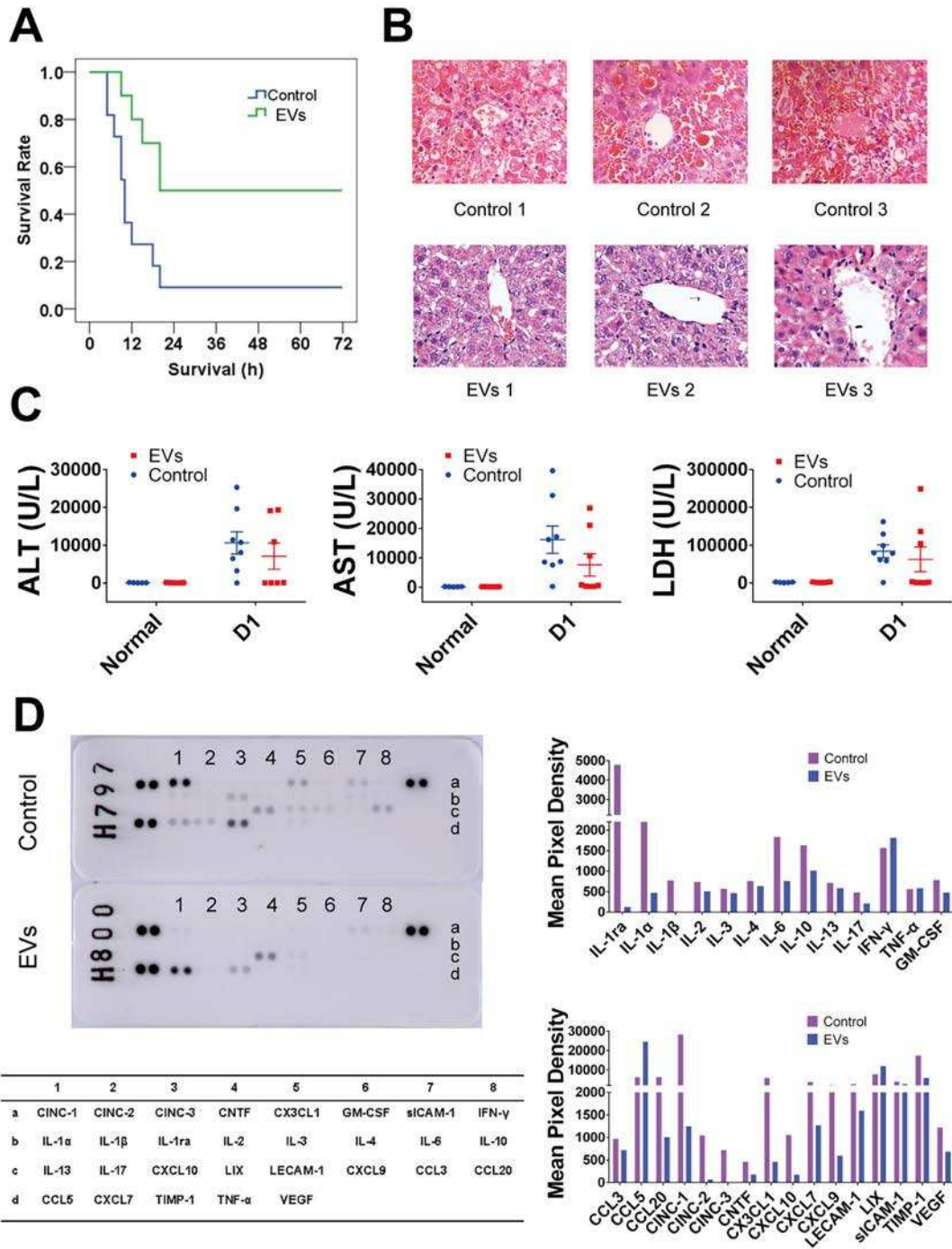
Fig. 4. hASCs-derived EVs rescue D-gal + LPS induced ALF. (A) When a comparison was made between the high-concentration EVs transplantation group and control group, the survival rates at different time points presented significant differences ($P < 0.05$). (B) At 24 h after the transplantation, the paraffin sections of the liver tissues of rats in each group were prepared, and photos were taken under a microscope after HE staining (400×). (C) At 24 h after transplantation, the rats in the high-concentration hASCs-derived EVs transplantation group had a significantly higher level of ALT, AST and LDH than those in the control group ($P < 0.05$). (D) As was shown in the protein chip detection, at 1 day after transplantation, the rats in the high-concentration hASCs-derived EVs transplantation group had a significantly lower level of inflammatory factors in the rat serum than those in the PBS control group, as well as a significantly lower level of chemotactic factors than those in the PBS control group.

after treatment with AZD6094, and the AZD6094-EVs group has the lowest expression quantity of c-Met, which may be caused by the role of AZD6094 in restraining c-Met (Fig. S3H).

4. Discussion

Over the recent years, some researchers considered that stem cells used in cell therapy may trigger the body's rejection reaction and cause embolization, even death. While extracellular vesicles, a kind of particle in nanoscale containing a rich variety of proteins and nucleic acids, are apparently easier to be transported and perform their functions without the potential risk of embolism, and have a better performance in safety compared with stem cells by minimizing the potential risk to trigger innate and adaptive immune response. Moreover, the collected extracellular vesicles are also easier to preserve without losing their activities.

Stem cells-derived EVs can be involved in immunoregulation, promotion of vasculogenesis and impaired tissue's proliferation, reduction of inflammatory reactions and apoptosis etc. [31–37] through carrying a large amount of packaged proteins and RNAs. Due to EVs' intrinsic targeting characteristics, cargo proteins and RNA could be delivered directly to the recipient cells. As a natural cell product, they can avoid the phagocytosis or degradation of recipient macrophages and in vivo lysosome degradation, making it possible to circulate in vivo for extended periods [38, 39]. In addition, EVs can penetrate the blood-brain barrier which is difficult for many drugs to penetrate [40, 41]. Therefore, stem cells-derived EVs could be isolated in vitro and delivered to the recipient for disease treatment [7, 42–46].

In recent years, many researchers have applied stem cells-derived EVs to treat liver diseases. Hirata et al. utilized a conditioned medium of dental pulp stem cells to treat mice with liver fibrosis, and discovered that it could inhibit the expression of the inflammatory mediator, induce the apoptosis of activated hepatic stellate cells and play positive roles in the treatment of liver fibrosis [47]. The study of Tan et al. revealed that the EVs of mesenchymal stem cells can promote the hepatocellular regeneration of CCL4-induced liver fibrosis in mice and reduce hepatocellular apoptosis through activating the IL-6/STAT3 pathway. The manifestations included the high expression of the proliferating cell nuclear antigen (PCNA), cell cycle protein D1, anti-apoptosis gene Bcl-xL, and signal transduction and transcriptional activation factor 3 (STAT3) [24]. In addition, stem cell-derived EVs have protective effects on lipopolysaccharide (LPS), thioacetamide and radiation-induced acute liver injuries. Stem cell-derived EV transplantation may become a new treatment method for various kinds of acute liver injuries [4, 48–53].

Our research group validated the efficacy of hASCs-derived EVs in rat models of ALF induced by D-gal. The rats in the high-concentration and low-concentration hASCs-derived EVs groups had significantly higher 72-hour survival rates (100% and 62.5% respectively) than those in the PBS control group (27.3%). It is worth noting that there was no significant difference between the high-concentration and low-concentration lysate groups and the control group, which further shows that the hASCs exerted effects mainly through the EVs they released rather than through the hASCs themselves. To explore the mechanism for treating ALF using hASCs-derived EVs, we carried out RNA sequencing on post-transplantation rats' liver tissues and found an up-regulation of genes related to the coagulation function and drug metabolism pathways of the rats in the high concentration hASCs-derived EVs group. Therefore, we assumed that hASCs-derived EVs transplantation improved the in vivo status of the coagulation hypofunction of ALF rats and accelerated the D-gal metabolism process. Moreover, there was a down-regulation of genes related to signal pathways, which echoed the results obtained in our ALF rat models induced by D-gal + LPS. This indicates that hASCs-derived EVs could effectively inhibit the expression of inflammatory mediators.

In addition, there was an up-regulation in the human-derived long-chain non-coding RNA (lncRNA) H19 gene measured in the rats' livers in the hASCs-derived EVs group. We used software to predict the microRNA that might interact with human lncRNA H19, and found that lncRNA H19 happened to be closely associated with the microRNA of coagulation functions, drug metabolism, etc. pathways. In the previous RNA sequencing results, we also found an up-regulation in genes related to the coagulation function and drug metabolic pathways in rats' livers. As such, we assumed that human hASCs-derived EVs inhibited the expression of microRNA related to the coagulation function, drug metabolism, etc. pathways in rat liver tissues, thereby up-regulating such pathways and improving the survival rate of rats with ALF.

H19 is a non-coded RNA with a known length of 2.3 kb, its expression in the liver is active but decreases rapidly after the birth of an individual. Youhei et al. detected the expression of the H19 gene in different time segments in liver regeneration models in which most of the rat and mouse livers were resected, and found that H19 expression increased significantly in tissues with active hepatocellular proliferation; apparently, H19 plays an indispensable role in the regeneration of liver tissues and the initiation of proliferation [54, 55]. Our research group indicated that among the rats receiving injections of hASCs-derived EVs via the iliac vein, those receiving hASCs-derived EVs, hASCs-derived EVs with the H19 gene silenced and PBS had 72-hour overall survival rates of 100%, 40% and 10% respectively; the rats in the hASCs-derived EVs group and the hASCs-derived EVs with silenced H19 gene group presented significant differences in terms of the survival rates at different time points, indicating that lncRNA H19 could improve the survival rate of rats through hepatocellular proliferation. The in vitro Cell Counting Kit-8 (CCK8) test also validated that H19-silencing EVs derived from hASCs could reduce the proliferation promotion effects on human hepatocytes.

To verify the effectiveness of the EVs in a more severe and fatal ALF model, we adopted a more severe model of inflammation induced by D-gal + LPS and found that the rats in the hASCs-derived EVs group had a significantly higher 72-hour survival rate (50%) than those in the PBS control group (9%). To observe the inflammatory status in the rats' livers, we used the protein chip method to detect the inflammatory factors and chemokines in the rat serum. The hASCs-derived EVs transplantation group had a lower level of such inflammatory factors as IL-1ra, IL-1α, IL-1β, IL-6 and IL-17 than those in the PBS control group, as well as a lower level of such chemotactic factors as CCL20, CINC-1, CINC-2α/β, CINC-3, CNTF, CX3CL1, CXCL7, CXCL9, CXCL10 and LECAM-1 than those in the PBS control group. Our results indicated that hASCs-derived EVs can simultaneously down-regulate the expression of inflammatory mediators and chemotactic factors, relieve the degree of liver tissue necrosis and further improve the survival rate of ALF rats.

From the RNA sequencing analysis above, we also found an up-regulation of HGF/c-Met pathway and this was verified in the liver tissue of rats using RT-qPCR method. HGF/c-Met pathway is a well-known pathway associated to cells proliferation. To clearly know whether lncRNA H19 promotes hepatocyte regeneration via the HGF/c-Met pathway, we used AAV with an overexpression of lncRNA H19 to infect hASCs and subsequently collected its EVs. It was discovered that, whether in vitro or in vivo, the use of EVs with an overexpression of H19 can further enhance the promotion role of EVs in hepatocytes' proliferation and restrain hepatocyte apoptosis, and the HGF/c-Met pathway and such related downstream pathways as PI3K/AKT and STAT3 were all up-regulated, which hints that H19 can further enhance the role of hASCs-derived EVs in promoting hepatocytes' proliferation. Then the c-met inhibitor — AZD6094 was used to block HGF/c-Met pathway in hepatocytes. After pretreatment with AZD6094, hASCs-derived EVs lost their effect on promoting hepatocytes' proliferation, the rats' survival rate was reduced and the experiments in vivo and vitro all indicate that the EVs had a reduced role in promoting hepatocytes' proliferation and protecting apoptotic hepatocytes, and the expression of the HGF/c-Met channel and such related downstream channels as PI3K/AKT and STAT3 were down-regulated, which indicated that hASCs-derived EVs may promote hepatocytes' proliferation through the HGF/c-Met pathway and related downstream channels, thereby increasing the survival rate of rats with ALF.

Up to now, stem cells-derived EVs have increasingly attracted attentions from researchers due to the promising therapeutic effects in animal models with a variety of diseases. Undoubtedly, there is still much work to be done before those goals could be achieved, such as the establishment of the criteria to differentiate between different kinds of EVs, unification of the methodologies for exosome collection, the appropriate concentration and dosage for different conditions, the active ingredients and mechanism of exosome, and more importantly, the long-term efficacy and clinical safety.

ARTICLE IN PRESS

5. Conclusions

In summary, hASCs-derived EVs show potential therapeutic relevance in acute liver failure animal models. Our research group validated the efficacy of hASCs-derived EVs in acute liver failure and explored the role of lncRNA H19 through acute liver failure rat models induced by different drugs; the direct use of stem cells-derived EVs instead of the stem cells themselves is very likely to become a new method with potential for treating such liver diseases as liver fibrosis and acute liver failure.

Authors' Contributions

YPJ and JYW contributed equally to this paper. YPJ and JYW designed, performed and analyzed the experiments, and wrote the manuscript; LYM and SEG performed the isolation and cultivation of hMSCs; HCL extracted and identified the hASCs-derived EVs; RFS, XLW, DJY, SEG, KN and LZ performed the animal experiments and contributed to the acquisition of data; XW, XJW and CWC analyzed the data and edited the manuscript; and QCF, JX and ZLG coordinated the project, analyzed the experiments and wrote the manuscript.

Conflict of Interest

This manuscript is a previously unpublished work and no other submission or publication will be made. All of the authors participated in the study and they have agreed to the content of the manuscript and declared no conflict of interest.

Appendix A. Supplementary data

Supplementary data to this article can be found online at https://doi.org/10.1016/j.ebiom.2018.07.015.

References

[1] O'Grady, J., 2014]. Timing and benefit of liver transplantation in acute liver failure. J Hepatol 60, 663–670.

[2] Farkas, S., Hackl, C., Schlitt, H.J., 2014]. Overview of the indications and contraindications for liver transplantation. Cold Spring Harb Perspect Med 4.

[4] Chen, G., Jin, Y., Shi, X., Qiu, Y., Zhang, Y., Cheng, M., et al., 2015]. Adipose-derived stem cell-based treatment for acute liver failure. Stem Cell Res Ther 6, 40.

[5] Haga, H., Yan, I.K., Takahashi, K., Matsuda, A., Patel, T., 2017]. Extracellular vesicles from bone marrow-derived mesenchymal stem cells improve survival from lethal liver failure in mice. Stem Cells Transl Med 6, 1262–1272.

[7] Wang, J., Cen, P., Chen, J., Fan, L., Li, J., Cao, H., et al., 2017]. Role of mesenchymal stem cells, their derived factors, and extracellular vesicles in liver failure. Stem Cell Res Ther 8, 137.

[8] Pascual-Miguelanez, I., Salinas-Gomez, J., Fernandez-Luengas, D., Villar-Zarra, K., Clemente, L.V., Garcia-Arranz, M., et al., 2015]. Systemic treatment of acute liver failure with adipose derived stem cells. J Invest Surg 28, 120–126.

[9] Gilsanz, C., Aller, M.A., Fuentes-Julian, S., Prieto, I., Blazquez-Martinez, A., Argudo, S., et al., 2017]. Adipose-derived mesenchymal stem cells slow disease progression of acute-on-chronic liver failure. Biomed Pharmacother 91, 776–787.

[10] Pittenger, M.F., Mackay, A.M., Beck, S.C., Jaiswal, R.K., Douglas, R., Mosca, J.D., et al., 1999]. Multilineage potential of adult human mesenchymal stem cells. Science 284, 143–147.

[11] Lin, J.S., Zhou, L., Sagayaraj, A., Jumat, N.H., Choolani, M., Chan, J.K., et al., 2015]. Hepatic differentiation of human amniotic epithelial cells and in vivo therapeutic effect on animal model of cirrhosis. J Gastroenterol Hepatol 30, 1673–1682.

[12] Cao, H., Yang, J., Yu, J., Pan, Q., Li, J., Zhou, P., et al., 2012]. Therapeutic potential of transplanted placental mesenchymal stem cells in treating Chinese miniature pigs with acute liver failure. BMC Med 10, 56.

[13] Kim, S.J., Park, K.C., Lee, J.U., Kim, K.J., Kim, D.G., 2011]. Therapeutic potential of adipose tissue-derived stem cells for liver failure according to the transplantation routes. J Korean Surg Soc 81, 176–186.

[14] Griffin, M.D., Ryan, A.E., Alagesan, S., Lohan, P., Treacy, O., Ritter, T., 2013]. Anti-donor immune responses elicited by allogeneic mesenchymal stem cells: what have we learned so far? Immunol Cell Biol 91, 40–51.

[15] Ong, H.T., Redmond, S.L., Marano, R.J., Atlas, M.D., von Unge, M., Aabel, P., et al., 2017]. Paracrine activity from adipose-derived stem cells on in vitro wound healing in human tympanic membrane keratinocytes. Stem Cells Dev 26, 405–418.

[16] Yong, K.W., Li, Y., Liu, F., Bin, G., Lu, T.J., Wan, A.W., et al., 2016]. Paracrine effects of adipose-derived stem cells on matrix stiffness-induced cardiac myofibroblast differentiation via angiotensin II type 1 receptor and Smad7. Sci Rep 6, 33067.

[17] Motavaf, M., Pakravan, K., Babashah, S., Malekvandfard, F., Masoumi, M., Sadeghizadeh, M., 2016]. Therapeutic application of mesenchymal stem cell-derived exosomes: a promising cell-free therapeutic strategy in regenerative medicine. Cell Mol Biol (Noisy-le-Grand) 62, 74–79.

[18] Dai, M., Yu, M., Zhang, Y., Tian, W., 2017]. Exosome-like vesicles derived from adipose tissue provide biochemical cues for adipose tissue regeneration. Tissue Eng Part A 23, 1221–1230.

[19] Lee, M., Ban, J.J., Kim, K.Y., Jeon, G.S., Im, W., Sung, J.J., et al., 2016]. Adipose-derived stem cell exosomes alleviate pathology of amyotrophic lateral sclerosis in vitro. Biochem Biophys Res Commun 479, 434–439.

[20] Patel, R.S., Carter, G., El, B.G., Patel, A.A., Cooper, D.R., Murr, M., et al., 2016]. Adipose-derived stem cells from lean and obese humans show depot specific differences in their stem cell markers, exosome contents and senescence: role of protein kinase C delta (PKCdelta) in adipose stem cell niche. Stem Cell Investig 3, 2.

[21] Timmers, L., Lim, S.K., Arslan, F., Armstrong, J.S., Hoefer, I.E., Doevendans, P.A., et al., 2007]. Reduction of myocardial infarct size by human mesenchymal stem cell conditioned medium. Stem Cell Res 1, 129–137.

[22] Aslam, M., Baveja, R., Liang, O.D., Fernandez-Gonzalez, A., Lee, C., Mitsialis, S.A., et al., 2009]. Bone marrow stromal cells attenuate lung injury in a murine model of neonatal chronic lung disease. Am J Respir Crit Care Med 180, 1122–1130.

[23] Cheng, K., Rai, P., Plagov, A., Lan, X., Kumar, D., Salhan, D., et al., 2013]. Transplantation of bone marrow-derived MSCs improves cisplatinum-induced renal injury through paracrine mechanisms. Exp Mol Pathol 94, 466–473.

[24] Tan, C.Y., Lai, R.C., Wong, W., Dan, Y.Y., Lim, S.K., Ho, H.K., 2014]. Mesenchymal stem cell-derived exosomes promote hepatic regeneration in drug-induced liver injury models. Stem Cell Res Ther 5, 76.

[25] Li, T., Yan, Y., Wang, B., Qian, H., Zhang, X., Shen, L., et al., 2013]. Exosomes derived from human umbilical cord mesenchymal stem cells alleviate liver fibrosis. Stem Cells Dev 22, 845–854.

[26] Hyun, J., Wang, S., Kim, J., Kim, G.J., Jung, Y., 2015]. MicroRNA125b-mediated Hedgehog signaling influences liver regeneration by chorionic plate-derived mesenchymal stem cells. Sci Rep 5, 14135.

[27] Ko, S.F., Yip, H.K., Zhen, Y.Y., Lee, C.C., Lee, C.C., Huang, C.C., et al., 2015]. Adipose-derived mesenchymal stem cell exosomes suppress hepatocellular carcinoma growth in a rat model: apparent diffusion coefficient, natural killer T-cell responses, and histopathological features. Stem Cells Int 2015, 853506.

[28] Lou, G., Song, X., Yang, F., Wu, S., Wang, J., Chen, Z., et al., 2015]. Exosomes derived from miR-122-modified adipose tissue-derived MSCs increase chemosensitivity of hepatocellular carcinoma. J Hematol Oncol 8, 122.

[29] Fiore, E.J., Bayo, J.M., Garcia, M.G., Malvicini, M., Lloyd, R., Piccioni, F., et al., 2015]. Mesenchymal stromal cells engineered to produce IGF-I by recombinant adenovirus ameliorate liver fibrosis in mice. Stem Cells Dev 24, 791–801.

[30] Borrelli, D., Yankson, K., Shukla, N., Vilanilam, G., Ticer, T., Wolfram, J., 2018]. Extracellular vesicle therapeutics for liver disease. J Control Release 273, 86–98.

[31] Kinnaird, T., Stabile, E., Burnett, M.S., Epstein, S.E., 2004]. Bone-marrow-derived cells for enhancing collateral development: mechanisms, animal data, and initial clinical experiences. Circ Res 95, 354–363.

[32] Dorronsoro, A., Robbins, P.D., 2013]. Regenerating the injured kidney with human umbilical cord mesenchymal stem cell-derived exosomes. Stem Cell Res Ther 4, 39.

[33] Shi, R., Jin, Y., Cao, C., Han, S., Shao, X., Meng, L., et al., 2016]. Localization of human adipose-derived stem cells and their effect in repair of diabetic foot ulcers in rats. Stem Cell Res Ther 7, 155.

[34] Thery, C., Zitvogel, L., Amigorena, S., 2002]. Exosomes: composition, biogenesis and function. Nat Rev Immunol 2, 569–579.

[35] Nakagami, H., Maeda, K., Morishita, R., Iguchi, S., Nishikawa, T., Takami, Y., et al., 2005]. Novel autologous cell therapy in ischemic limb disease through growth factor secretion by cultured adipose tissue-derived stromal cells. Arterioscler Thromb Vasc Biol 25, 2542–2547.

[36] Kourembanas, S., 2015]. Exosomes: vehicles of intercellular signaling, biomarkers, and vectors of cell therapy. Annu Rev Physiol 77, 13–27.

[37] Togel, F., Hu, Z., Weiss, K., Isaac, J., Lange, C., Westenfelder, C., 2005]. Administered mesenchymal stem cells protect against ischemic acute renal failure through differentiation-independent mechanisms. Am J Physiol Ren Physiol 289, F31–F42.

[38] Hood, J.L., San, R.S., Wickline, S.A., 2011]. Exosomes released by melanoma cells prepare sentinel lymph nodes for tumor metastasis. Cancer Res 71, 3792–3801.

[39] Tan, A., Rajadas, J., Seifalian, A.M., 2013]. Exosomes as nano-theranostic delivery platforms for gene therapy. Adv Drug Deliv Rev 65, 357–367.

[40] Ha, D., Yang, N., Nadithe, V., 2016]. Exosomes as therapeutic drug carriers and delivery vehicles across biological membranes: current perspectives and future challenges. Acta Pharm Sin B 6, 287–296.

[41] Chen, C.C., Liu, L., Ma, F., Wong, C.W., Guo, X.E., Chacko, J.V., et al., 2016]. Elucidation of exosome migration across the blood-brain barrier model in vitro. Cell Mol Bioeng 9, 509–529.

[42] Sullivan, R., Maresh, G., Zhang, X., Salomon, C., Hooper, J., Margolin, D., et al., 2017]. The emerging roles of extracellular vesicles as communication vehicles within the tumor microenvironment and beyond. Front Endocrinol (Lausanne) 8, 194.

[43] Chen, J.J., Zhao, B., Zhao, J., Li, S., 2017]. Potential roles of exosomal microRNAs as diagnostic biomarkers and therapeutic application in Alzheimer's disease. Neural Plast 2017, 7027380.

[44] Rufino-Ramos, D., Albuquerque, P.R., Carmona, V., Perfeito, R., Nobre, R.J., Pereira, D.A.L., 2017]. Extracellular vesicles: novel promising delivery systems for therapy of brain diseases. J Control Release 262, 247–258.

[45] Wang, J., Sun, X., Zhao, J., Yang, Y., Cai, X., Xu, J., et al., 2017]. Exosomes: a novel strategy for treatment and prevention of diseases. Front Pharmacol 8, 300.

[46] Dykes, I.M., 2017]. Exosomes in cardiovascular medicine. Cardiol Ther 6, 225–237.

[47] Hirata, M., Ishigami, M., Matsushita, Y., Ito, T., Hattori, H., Hibi, H., et al., 2016]. Multifaceted therapeutic benefits of factors derived from dental pulp stem cells for mouse liver fibrosis. Stem Cells Transl Med 5, 1416–1424.

[48] Zhang, Y., Cai, W., Huang, Q., Gu, Y., Shi, Y., Huang, J., et al., 2014]. Mesenchymal stem cells alleviate bacteria-induced liver injury in mice by inducing regulatory dendritic cells. Hepatology 59, 671–682.

[49] Quintanilha, L.F., Takami, T., Hirose, Y., Fujisawa, K., Murata, Y., Yamamoto, N., et al., 2014]. Canine mesenchymal stem cells show antioxidant properties against thioacetamide-induced liver injury in vitro and in vivo. Hepatol Res 44, E206–E217.

[50] Fu, J., Zhang, H., Zhuang, Y., Liu, H., Shi, Q., Li, D., et al., 2014]. The role of N-acetyltransferase 8 in mesenchymal stem cell-based therapy for liver ischemia/reperfusion injury in rats. PLoS One 9, e103355.

[51] Zhang, J., Zhou, S., Zhou, Y., Feng, F., Wang, Q., Zhu, X., et al., 2014]. Hepatocyte growth factor gene-modified adipose-derived mesenchymal stem cells ameliorate radiation induced liver damage in a rat model. PLoS One 9, e114670.

[52] van Poll, D., Parekkadan, B., Cho, C.H., Berthiaume, F., Nahmias, Y., Tilles, A.W., et al., 2008]. Mesenchymal stem cell-derived molecules directly modulate hepatocellular death and regeneration in vitro and in vivo. Hepatology 47, 1634–1643.

[53] Chen, Y.X., Zeng, Z.C., Sun, J., Zeng, H.Y., Huang, Y., Zhang, Z.Y., 2015]. Mesenchymal stem cell-conditioned medium prevents radiation-induced liver injury by inhibiting inflammation and protecting sinusoidal endothelial cells. J Radiat Res 56, 700–708.

[54] Wang, S., Wu, X., Liu, Y., Yuan, J., Yang, F., Huang, J., et al., 2016]. Long noncoding RNA H19 inhibits the proliferation of fetal liver cells and the Wnt signaling pathway. FEBS Lett 590, 559–570.

[55] Yamamoto, Y., Nishikawa, Y., Tokairin, T., Omori, Y., Enomoto, K., 2004]. Increased expression of H19 non-coding mRNA follows hepatocyte proliferation in the rat and mouse. J Hepatol 40, 808–814.

Further-reading

[3] Olivo, R., Guarrera, J.V., Pyrsopoulos, N.T., 2018]. Liver transplantation for acute liver failure. Clin Liver Dis 22, 409–417.

[6] Wang, J., Ren, H., Yuan, X., Ma, H., Shi, X., Ding, Y., 2018]. Interleukin-10 secreted by mesenchymal stem cells attenuates acute liver failure through inhibiting pyroptosis. Hepatol Res 48, E194–E202.